

# SCIENTIFIC REPORTS



OPEN

## Live *E. coli* bacteria label-free sensing using a microcavity in-line Mach-Zehnder interferometer

Monika Janik<sup>1</sup>, Marcin Koba<sup>2,3</sup>, Anna Celebańska<sup>1</sup>, Wojtek J. Bock<sup>1</sup> & Mateusz Śmietana<sup>3</sup>

The paper presents the first study to date on selective label-free biosensing with a microcavity in-line Mach-Zehnder interferometer induced in an optical fiber. The sensing structures were fabricated in a single-mode fiber by femtosecond laser micromachining. In contrast to other studies of this sensing scheme, where only the sensitivity to refractive index changes in the cavity was investigated, this research used chemical surface treatment of the sensor to ensure detection specificity. Immobilized MS2 bacteriophages were applied as recognition elements specifically targeting live *E. coli* C3000 bacteria. It is shown that the sensor allows for real-time monitoring of biological phenomena taking place on the surface of the microcavity. The developed biosensor exhibits ultrahigh refractive index sensitivity of 15,000 nm/RIU and is capable of detecting live *E. coli* bacteria concentrations as low as 100 colony forming units (CFU)/mL in liquid volume as low as picoliters.

Nowadays early and fast pathogenic detection and identification are crucial, e.g., for patients' examinations in hospitals, especially those with sepsis<sup>1</sup> or infections, where the strain of bacteria has to be identified as soon as possible to find the best suitable treatment. They are also needed for diagnosis of the state of water reservoirs, biomedical research, as well as for safety in the food industry and environmental monitoring. Bacterial infections cause several millions of diseases worldwide each year<sup>2</sup>. Thus, researchers focus on biosensors directly detecting whole bacteria cells, rather than isolated biological components, e.g., enzymes<sup>3</sup>, lipopolysaccharides<sup>4</sup>, or outer membrane proteins<sup>5</sup>. This approach has several advantages: whole cells are more tolerant of environmental changes such temperature, pH, than isolated structures; Isolation of whole microorganisms from natural sources is very easy; There is no need of extensive preparation of the sample before measurements.

Currently, bacteria detection still relies mostly on classical microbiology methods including isolation and bacteria growth in selective media<sup>6</sup>. These techniques are very effective, but they require high technical skills and are time-consuming due to the slow process of microorganism culturing. Therefore, there is an urgent need to develop alternative bacteria detection methods. Over recent years, biosensor development tackled this problem and has adopted numerous modern approaches including polymerase chain reaction (PCR), genomic sequencing, mass spectrometry, and microarrays. However, these methods involve sophisticated and expensive equipment, require high technical skills and complicated multi-step sample preparation and post-processing.

To overcome limitations of existing technology a new biosensor needs to be highly sensitive, specific, cost-effective, compact and easy to use. Based on these expectations, optical fiber sensors can be a compelling alternative to conventional analytical techniques. These sensors have many advantages including immunity to electromagnetic interference, real-time detection, the possibility of multiplexing, and high resistance to harsh environmental conditions. A number of compact optical fiber sensors have been reported, including devices based on long-period fiber gratings (LPFGs)<sup>7</sup>, fiber Bragg gratings (FBG)<sup>8</sup>, and photonic crystal fiber (PC)<sup>9</sup>. LPFGs were shown to be especially effective for bacteria detection<sup>4,10,11</sup>. It is notable that in most of the studies, killed bacteria were applied instead of vivid microorganisms. Although the LPFG is compact and limits of detection (LOD) have been reported as low as 10<sup>2</sup> Colony Forming Units (CFU)/mL<sup>12</sup>, this type of sensor with 5–6 cm length usually requires at least 500 µL of examined sample.

Since in most biological and chemical analysis only limited volumes of samples are available, therefore, significant attention has been focused on structures based on in-fiber microcavities. One of the reported devices is

<sup>1</sup>Photonics Research Center, Université du Québec en Outaouais, 101 Rue St Jean Bosco, Gatineau, QC, J8X 3x7, Canada. <sup>2</sup>The National Institute of Telecommunications, Szachowa 1, Warszawa, 04-894, Poland. <sup>3</sup>The Institute of Microelectronics and Optoelectronics, Warsaw University of Technology, Koszykowa 75, Warszawa, 00-662, Poland. Correspondence and requests for materials should be addressed to M.J. (email: [monikaa.janik@gmail.com](mailto:monikaa.janik@gmail.com))

microcavity in-line Mach-Zehnder interferometer ( $\mu$ IMZI)<sup>13</sup>. The structure is constituted by a small and deep hole, micro-machined in a single-mode optical fiber. Light propagating through the fiber core splits at the cavity's sidewall into two parts – one propagates in the core, and the other penetrates the cavity. The beams interfere with the second wall of the cavity. In this sensing scheme, the investigated media can directly interact with the fiber core. The  $\mu$ IMZI device offers very high refractive index (RI) sensitivity reaching over 20,000 nm/RIU, making it one of the most RI-sensitive devices to date<sup>14</sup>. Due to very precise fabrication, the device is small, highly reproducible, and portable. Moreover, it is temperature-insensitive<sup>15</sup>, which is essential since temperature is one of the most disrupting factors in RI measurements. Along with an examination of ultra-small volume samples, the  $\mu$ IMZI can certainly be used for label-free sensing concept. This concept relies mainly on changes in optical properties at the sensor's surface. In comparison to fluorescent-based detection, in the label-free protocol, there is no need to use special tags or labeling, what enables us to detect the biological molecules in their natural form. Hence label-free sensing is usually cheaper, faster and easier to perform.

Some highly sensitive sensors based on  $\mu$ IMZIs have been proposed for sensing strain<sup>16</sup>, pressure<sup>17</sup> and RI<sup>14</sup>, but never for specific biosensing, including bacteria detection. Recently Li *et al.* reported bovine serum albumin (BSA)  $\mu$ IMZI-based biosensor<sup>18</sup>. Although, the sensor exhibited high RI sensitivity reaching 10,000 nm/RIU, and the low detection limit, the specific receptor has not been applied. Thus, the recorded spectrum dependent on the RI of BSA solution which changes tighter with its concentration.

To adapt a device for pathogen detection, the sensor's surface must be specially modified. One of the crucial steps for the efficiency of a biosensor is the choice of bioreceptor. The bioreceptor can have an impact on the sensitivity and can make the sensor specific towards the chosen bacterial target. To date, a broad spectrum of bioreceptors has been used for bacterial detection, including antibodies<sup>19</sup>, sugars/lectins<sup>20</sup>, proteins<sup>4,11</sup>, aptamers<sup>21</sup>, and phages<sup>7,22</sup>. Each of these recognition elements has its advantages and disadvantages. In particular, bacteriophages can be highly specific towards bacteria, are cost-effective, have a long shelf-life, and exhibit high thermal stability. Until now, T4 bacteriophages have been the leading choice for application on an LPFG for *E. coli* detection<sup>7,22</sup>. However, the MS2 bacteriophage is also known to infect the male *E. coli* bacterium. This virus has already been immobilized on an LPFG-based biosensor<sup>12</sup>. Due to the lysogenic cycle of MS2<sup>23</sup> - which does not result in immediate destruction of the host cell in comparison to the T4 phage - at controlled conditions stable measurements were possible. Furthermore, its simple structure compared to the T4 phage assures that the phage is well-orientated on the fiber surface, what was very challenging in the case of the T4 application.

In this work, we present for the first time a bacteria-specific  $\mu$ IMZI-based label-free biosensor. The measurements are performed using different concentrations of live *E. coli* C3000 as well as bacteria dry weight. The MS2 phages are immobilized on the functionalized surface as specific recognition elements. This paper shows that besides tracking the changes in the RI of the liquid filling the cavity, the  $\mu$ IMZI-based sensor can also simultaneously investigate the phenomena taking place at its surface.

## Materials and Methods

**$\mu$ IMZI fabrication and analysis.** Structures in the form of cylindrical cavities with a diameter ( $d$ ) of 50  $\mu$ m were fabricated in standard Corning SMF28e fibers following the method described in<sup>14</sup>. In order to identify the response of the structures to a thin high-RI film, such as biological film on the cavity surface, a set of  $\mu$ IMZIs was coated by atomic layer deposition (ALD) with a high-RI aluminum oxide ( $\text{Al}_2\text{O}_3$ ) film according to the procedure reported in<sup>24</sup>. The  $\text{Al}_2\text{O}_3$  thickness reached  $t = 154$  nm. The use of a nano-coating with a high-RI material made it possible to simulate the effects of biofilm formation. The deposition was followed by slow chemical etching of the film using 10 mM sodium hydroxide (NaOH) (Sigma-Aldrich) at 20 °C for a specific time, and the optical response was verified after extensive cavity washing with deionized water. During the entire process, the  $\mu$ IMZI transmission was monitored with an NKT Photonics SuperK COMPACT supercontinuum white light source and a Yokogawa AQ6370C optical spectrum analyzer in the spectral range of 1100–1700 nm. A set of water/glycerin solutions with RI varied in the range of  $n_D = 1.3330$ – $1.3900$  RIU was used to perform the reference RI sensitivity measurements. The RI of the solutions was measured using a digital refractometer VEE GEE PDX-95.

**Preparation of biological samples.** All the bacteria strains, as well as the MS2 bacteriophages used in described experiments, were obtained from the INRS-Institute Armand-Frappier Research Center, where were prepared following the procedure described in<sup>23</sup>.

**Biofunctionalization of the  $\mu$ IMZI.** In the first step of the functionalization of the surface, the cavity was cleaned with a mixture of hydrochloric acid and methanol (1:1, v/v) (Sigma-Aldrich) for 30 minutes and then in sulfuric acid (Sigma-Aldrich) (30 minutes) to remove contaminations and to enhance the density of superficial hydroxyl groups (Si-OH)<sup>25</sup>. This step was completed by extensive rinsing with water and vacuum drying. In the next step, the silanization process was carried out from the (3-Aminopropyl) triethoxysilane (APTES) (Sigma-Aldrich) gas phase according to the modified procedure presented in<sup>26</sup>. The effectiveness of the process is controlled by exposure time or the amount of the precursor. The silanization was performed in a small vacuum desiccator filled with argon. Two trays of a 30  $\mu$ l of APTES and 10  $\mu$ l of triethylamine (Sigma-Aldrich) (a sol-gel process catalyst) were placed in the desiccator chamber and left for over 30 minutes. The vials were then removed, and the cavity was kept in an argon atmosphere for 48 hours for curing<sup>27</sup>. Next, the deposited amine groups were activated by the homo-bifunctional cross-linking agent glutaraldehyde (GLU) (Sigma-Aldrich) through immersion in 2.5% GLU solution in PBS for 30 minutes. The obtained surface was very sensitive to amine groups at the capsid of the bacteriophages. For the conjugation, the sensor was incubated in a phages solution for 1 hour, followed by immersion in 2 mg/mL BSA solution in PBS for 30 minutes in order to block non-specific interaction. In the last step, the sensor was exposed to the bacteria for 30 minutes. The  $\mu$ IMZI sensor with MS2 phages immobilized on the surface was used to detect different concentrations of live *E. coli* C3000 strain in solution (Fig. 1).

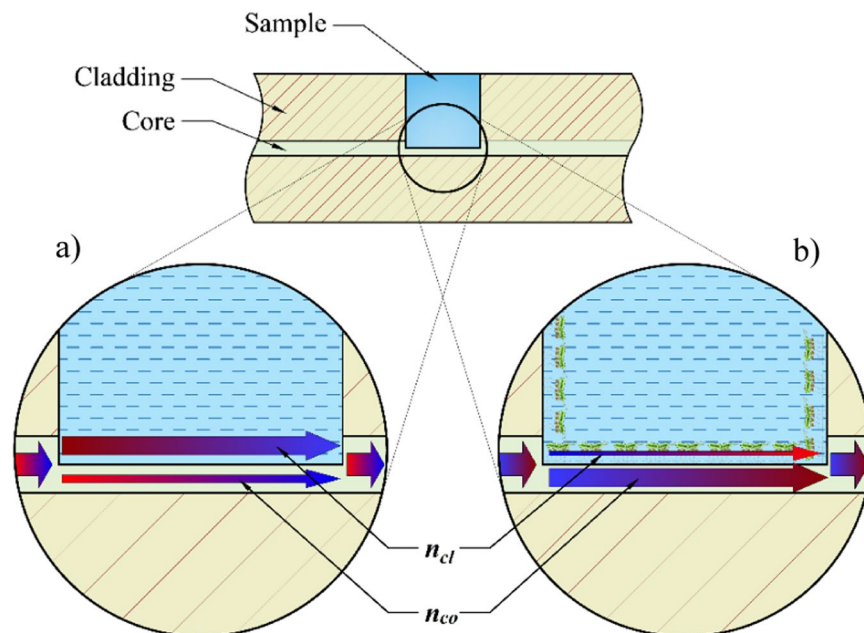


**Figure 1.** Schematically shown  $\mu$ IMZI structure and two interfering modes, namely  $n_{co}$ , and  $n_{cl}$  in the remaining part of the fiber core and micromachined circular cavity, respectively, influenced by A. the liquid inside the cavity and B. specifically bound bio-layer. The drawing is not to scale.

Bacteria dilutions in concentrations of  $10^2$ ,  $10^4$ ,  $10^6$ ,  $10^7$  and  $10^8$  CFU/mL in PBS were prepared. For selectivity measurements, a negative sample containing *B. Thailandensis* was prepared in a concentration of  $10^8$  CFU/mL. During experiments, the sensor was immersed in increasing concentration of C3000 strain for 30 minutes in each concentration. After the bacteria incubation, the sensor was extensively washed and measured in PBS to obtain reference results. The difference between wavelength corresponding to transmission minima after BSA binding and after each bacteria exposer was treated as the sensor response.

For determination of sensor's selectivity, the  $\mu$ IMZI after immobilization of the MS2 phage and blocking with BSA was immersed in a solution of a non-specific strain of bacteria for 30 minutes, then washed and measured in PBS. Another selectivity verification was performed using *E. coli* C3000 with no MS2 phage immobilized but only blocked with BSA to exclude unspecific binding between bacteria and the functionalized surface.

## Results and Discussion

**RI sensitivity of the  $\mu$ IMZI sensor.** Before measuring  $\mu$ IMZI with bacteria, we studied the response of the sensor to different RI filling the cavity and thicknesses of the thin high-RI film deposited inside the microcavity. Following the analysis presented in<sup>18,28</sup> and the Eq. (1) describing the spectral placement of the transmission minimum ( $\lambda_m$ ):

$$\lambda_m = \frac{2\pi d \Delta n_{eff}}{(2m + 1)\pi - \varphi_0}, \quad (1)$$

where  $\Delta n_{eff} = n_{co} - n_{cl}$  is the difference between the effective RI of the two interfering modes, namely  $n_{co}$ , and  $n_{cl}$  in the remaining part of the fiber core and micromachined circular cavity, respectively,  $d$  is the diameter of the microcavity, and  $\varphi_0$  represents initial phase, it can be stated that the difference  $\Delta n_{eff}$  is the main component responsible for the spectral shift of the pattern (i.e., transmission minimum). Two different effects can induce the changes in  $n_{eff}$ , namely changing the RI filling the cavity what corresponds mainly to  $n_{cl}$  or/and by the formation of an adlayer on the microcavity's surface what in turn mainly influences  $n_{co}$ . To investigate the response of the  $\mu$ IMZI to these two effects, reference measurements for different RI filling in the cavity and different thickness of the film on cavity surface were conducted (Fig. 2). In Fig. 2a is shown the effect of an increase in the RI in the microcavity. The transmission minima shift towards shorter wavelengths, and the RI sensitivity reaches 15,000 nm/RIU. In contrast, in Fig. 2b the response of the  $\mu$ IMZI to changes in thickness of a high-RI layer ( $Al_2O_3$ ) deposited inside the cavity is shown. It has been determined using spectroscopic ellipsometry that the etching rate of  $Al_2O_3$  reached  $\sim 0.65$  nm/min<sup>29</sup>. The RI of  $Al_2O_3$  is higher than that of either the fiber core or the cladding. Measurements were performed in water in consecutive time steps as shown in Fig. 2b. This figure illustrates that deposition of the thin layer caused a change in the depth of the resonance minimum from about  $-39$  dB to  $-24$  dB. Compared to the effect presented in Fig. 2a, the spectra do not change in a predictable, monotonic manner. During the first 10 minutes of the etching process, the transmission minimum shifts towards longer wavelengths. Later, as the thickness of the high-RI film decreases, a shift towards shorter wavelengths is observed.

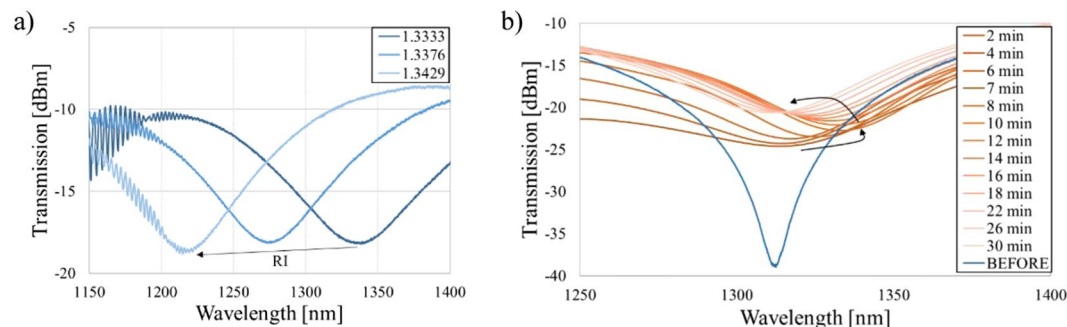


**Figure 2.** Transmission spectra of the  $\mu$ IMZI with the cavity diameter  $d = 50 \mu\text{m}$ , where (a) shows a response to RI changes and (b) shows the evolution of the  $\text{Al}_2\text{O}_3$  film thickness (initially  $t = 154 \text{ nm}$ ) with its etching process recorded for a water-filled cavity. The spectrum before the deposition was given for reference. Arrows indicate the shift of the minimum induced by each procedure.

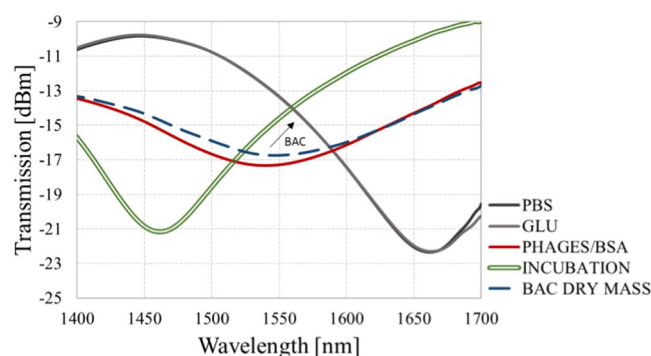


**Figure 3.** Transmission spectra of the  $\mu$ IMZI at each stage of the experiment with *E. coli* C3000 (1 mg/mL) dry weight. The arrow indicates the change induced by bacteria binding.

Depending on the  $\mu$ IMZI working conditions determined by the thin-film properties (mainly thickness and RI) and the depth of the microcavity, the effect of the changes in  $n_{co}$  manifests differently.

The results shown above indicate that both RI changes in the liquid and additional layer deposition have a significant influence on the  $\mu$ IMZI response. However, each of these parameters affects  $\Delta n_{eff}$  differently. When the RI of the liquid increases, the propagation conditions are affected primarily through the  $n_{cb}$ , while depositing a high-RI film on the core surface influences mainly the  $n_{co}$ <sup>28</sup>. This explains why we are observing the different behavior of the spectrum and allows us to interpret further results.

**Bacteria dry-weight sensing.** One of the most significant differences between live bacteria and bacteria dry weight is that the lyophilized cells have no motility. Along with the incubation during measurements, cells simply sediment and aggregate on the sensor surface. This makes them easier to detect than the live, motile pathogen. Therefore, we perform a preliminary experiment with lyophilized *E. coli* C3000.

As shown in Fig. 2a, the spectral response of the  $\mu$ IMZI strongly depends on the RI filling the microcavity. That is why each step of the biofunctionalization was followed by measurements in PBS after extensive washing of the cavity. The purpose of washing was to remove biological residues which were only physically attached to the functionalized surface and could have a disturbing impact on the measurement. To achieve the relative shift of the transmission minima, only measurements performed in the same solution (here PBS) were compared.

Figure 3 presents the transmission spectra obtained for each stage of the experiment, namely:

- (1) Functionalization of the surface, i.e., silanization with APTES (gas phase) (blue curve), where the process was controlled by exposure time and the amount of the precursor, followed by activation of the deposited amine groups by glutaraldehyde (GLU) (grey curve);
- (2) Immobilization of bioreceptor, i.e., MS2 phages and blocking the surface with BSA solution (red curve);
- (3) *E. coli* bacteria detection: incubation of the sensor in bacteria solution (green, double curve) and bacteria attached to the surface (blue, dashed curve).

Stage (1) for cavity filled with PBS can be considered as a baseline. What has been reported in<sup>30</sup> thick layers of silane are very fragile and may be washed away either in the presence of a buffer or during various washing steps in an assay process. Therefore, the functionalization process was optimized to obtain a thin and stable silane/GLU layer, that could not change the working conditions of the  $\mu$ IMZI (no spectral shift of the pattern after the

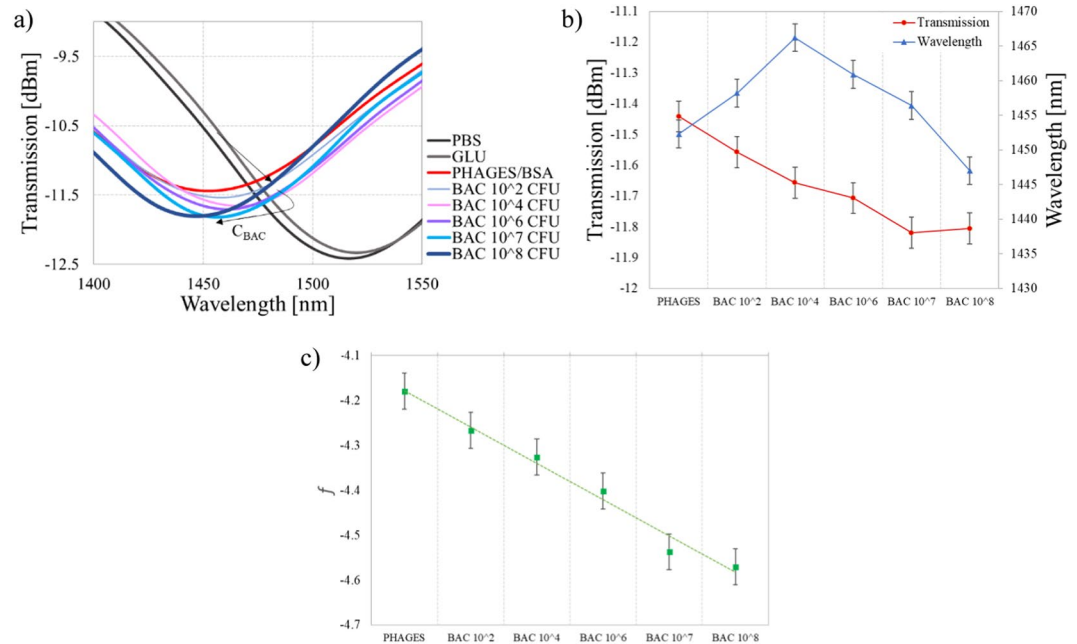


**Figure 4.** The response of the  $\mu$ IMZI at each stage of the experiment with different concentrations of live *E. coli* C3000 bacteria where (a) shows the transmission spectra in PBS after incubation and extensive washing and (b) shows a correlation between the transmission and the wavelength (c) shows linear combination between the transmission and the wavelength.

functionalization was noticed). On the other hand, the introduction of highly concentrated phages ( $10^9$  PFU/mL) (stage 2) with an average RI equal to 1.217 RIU<sup>31</sup> changed working conditions of the  $\mu$ IMZI through the formation of low RI adlayer and thus significantly affected the  $n_{co}$ . Presence of tens of nm thick layer had a significant influence on the spectrum, i.e., the minimum ( $\lambda_m$ ) strongly shifted towards lower wavelengths and decreased in depth from  $-23$  dB before phages immobilization to  $-17$  dB after the process. A similar effect can be observed in Fig. 2b, which shows how an additional layer caused a decrease in the intensity of the transmission. During the blocking step, the introduction of dense blocking solution (2 mg/mL) filled empty spaces and prevented from unspecific binding but did not introduce any further changes in  $\lambda_m$ . This may be caused by the very small size of BSA molecules and an already uniform (dense) layer of phages. After the sensor surface functionalization, it has been exposed to bacteria dry weight (1 mg/mL) (stage 3). As can be seen in the Fig. 3, the minimum shifts 7 nm towards longer wavelengths (the shift is designated by a blue, dashed line). Given that the observed change induced by bacteria cells was obtained after extensive washing with PBS, the shift must be influenced by the growth of the specific adlayer on the microcavity surface, not by a change in the RI of the solution as observed during bacteria incubation (designated by the double green line).

**Detection of live *E. coli*.** On the top of the lack of mobility, there are also other differences between killed and live microbes which can have an impact on measurement performance. After lyophilization, heat treatment or ultrasonication, the structural properties of bacteria cells are changed. Together with dehydration, changes may occur in the shape of the bacteria cell and in some of the surface structures, especially pili or fimbria, which are very important in the case of MS2-based detection. As a result, it is impossible to determine what has bonded to the surface – whole bacteria cells or some detached elements. Furthermore, during the sample preparation of killed microorganisms, bacteria cells can be destroyed, causing the release of internal structures such as proteins. This can also affect the optical responses. To imitate bacteria detection in their natural environment an experiment with live bacteria was conducted. Vivid bacteria are motile, in their proper shape, equipped with all the usual surface structures thus, makes measurements more challenging. A bilayer formed by live bacteria typically has different properties than layer previously created by bacteria dry-weight, including those optical. For example, it may contain air gaps due to the presence of fimbria/pili on the surface which holds the surface of the cells at a distance from the  $\mu$ IMZI bottom. Since immobilized MS2 are bound to the pili, this causes no problems with capturing bacteria and keeping them on the  $\mu$ IMZI surface. However, the layer can never be as dense and uniform as a layer formed by immobilized, killed bacteria or bacteriophages. What is more, the layer can scatter the light even more through the extremely rough surface of bacteria, what can lead to additional losses.

The spectra obtained at each stage of the experiment are shown in Fig. 4a. Even for concentration as low as 100 CFU/mL of bacteria, a 5.9 nm spectral shift can be observed. Especially noticeable is the fact that the spectrum shifts differently than during the previous experiment with killed bacteria, what could be expected due to the differences in bilayer properties mentioned above. Subsequent additions of the solutions with a higher concentration of *E. coli* C3000 caused further changes in the wavelength of the transmission minimum. It is worth to mention that the depth of the micromachined cavity is  $\sim 62 \mu\text{m}$ , so it is  $\sim 4 \mu\text{m}$  inside the core. Hence, a layer with

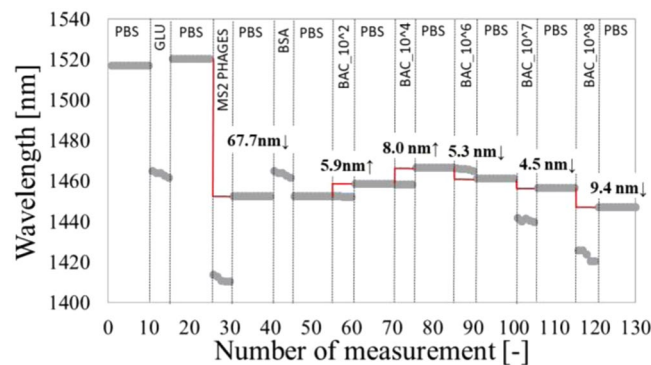


**Figure 5.** A shift of the minimum's wavelength at each stage of the experiment induced by functionalization and incubation in different concentrations of live bacteria.

the thickness of 4–5  $\mu\text{m}$  will affect  $n_{co}$  the most, creating new conditions for the light propagation inside the core. Further augmentation of the layer exceeding the 4  $\mu\text{m}$  thickness negligibly changes  $n_{co}$ , but, in contrast, affects  $n_{cl}$ . The addition of bacterial solutions with a concentration of up to  $10^4$  CFU/mL shifted the spectrum toward longer wavelengths. It is expected at this stage of the experiment that the  $n_{co}$  is mainly affected, while the RI of bacterial solution stays equal to 1.388 RIU<sup>32</sup>. Considering that the size of bacteria spans from 2  $\mu\text{m}$ <sup>23</sup> and the length of the fimbriae 1  $\mu\text{m}$ <sup>33</sup> – the last layer is the thickest one in the system. According to the MS2 infection cycle and place of attachment to the bacterium, we need to take into account that the layer of *E. coli* formed on the sensor surface can increase its density and thickness. Further growth of the adlayer, especially after incubation in a higher concentration of bacteria, affects mainly  $n_{cl}$ . Under these conditions according to the Eq. (1), the minimum's shift changes its direction towards shorter wavelengths. This mechanism explains non-monotonous response. This explanation stays in agreement with the previously presented response of the sensor to increase in  $\text{Al}_2\text{O}_3$  film thickness (Fig. 2b), where the response followed in the same non-monotonous scheme.

Despite the non-monotonous response and the initial position of the minimum, the following trials revealed the same trend in a shift of the minimum. For concentrations as small as  $10^2$ – $10^5$  CFU/ml we observed a gradual shift of the minimum towards longer wavelengths and increase of its depth. For higher concentrations –  $10^6$ – $10^8$  CFU/ml – the direction of the shift has changed towards shorter wavelengths, but its depth kept increasing. With a combination of these two parameters, i.e., the minimum's wavelength and transmission, the distinction between different concentrations of bacteria is possible (Fig. 4b). Furthermore, with a linear combination of the transmission and the wavelength which gives a monotonic function, it is possible to obtain an unambiguous mapping of the two values to specific bacteria concentration. An example of such linear combination can be Eq. 2:

$$f = A \cdot \text{Wavelength} + B \cdot \text{Transmission}, \quad (2)$$

where A and B are scaling factors expressed in [ $\text{nm}^{-1}$ ] and [ $\text{dBm}^{-1}$ ], respectively. The factors transform wavelength and transmission into the same range and guarantee the consistency of units. Function given in Eq. 2 with appropriate coefficients simplify the recognition of the bacteria concentration. As an example we can substitute  $A = 0.005$  and  $B = 1$ , the outcome is shown in Fig. 4c.

To assure that the obtained effects come from the formation of the biological layer and not from changes in the RI of the solution, the wavelength of the minimum after each stage of the biofunctionalization is plotted (Fig. 5). Due to higher  $n_{cl}$  present in the cavity during the functionalization process, e.g., incubation with GLU, the spectrum temporarily experienced shift towards lower wavelength. We can observe the same effect during incubation with, i.e., phages, or higher concentrations of bacteria ( $10^7$  and  $10^8$  CFU/mL). After extensive washing of the surface with PBS, the signal changes, revealing the influence of the adlayer.

The described sensor has shown superiority over the other fiber-optic platforms regarding sensitivity, easiness of fabrication, and the required volume of the sample. The similar assay strategies using APTES/GLU surface functionalization and phages were used for detection of other *E. coli* strains by employing LPFG<sup>7,22</sup>, FBG<sup>34</sup>, and multi-mode microfiber probe<sup>35</sup>. Although the detection limit of these probes reached  $10^3$  CFU/ml, sensitivities of those platforms were lower. The similar strategy using antibodies as a biorecognition element was used to detect other *E. coli* strains by employing plastic optical fiber<sup>36</sup>. It resulted in a LOD of  $10^3$  CFU/mL with a detection time of 10 minutes per sample, but a sample volume required for measurements was equal to 5–6 ml. The U-bent fiber optic probe<sup>37</sup> using immobilized antibodies was also developed for *E. coli* detection resulted in a LOD of  $10^3$  CFU/ml, using 500  $\mu\text{l}$  of the sample per measurement whereas our method was capable of detecting 100 CFU/ml in over ten times smaller volumes.

**Negative controls.** During the adsorption-based measurement, one might expect the *E. coli* bacteria to be easily wiped off the surface by subsequent PBS buffer washes. In the described experiments, however, they remained firmly attached to the fiber surface due to well oriented, immobilized phages. The shown spectral shift was therefore influenced mostly by the change in the thickness of the specific biolayer on the  $\mu\text{IMZI}$  surface. To prove this point, two negative control experiments were performed. In the first one to verify the selectivity of the bioreceptor, we used the *B. Thailandensis* strain, which shows no affinity to MS2. The second control experiment

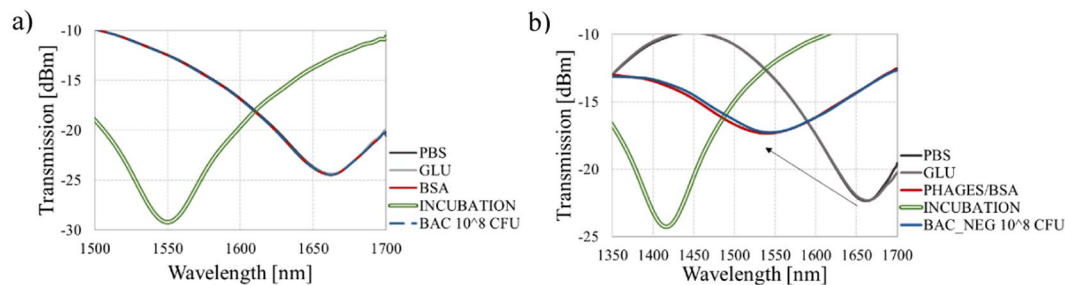


**Figure 6.** Transmission spectra of the  $\mu$ MZI at each of the stage of the experiment, showing the response (a) for positive *E. coli* C3000 without phages on the sensor's surface and (b) for negative *B. Thailandensis* with MS2 phages.

was performed with no MS2 phages but using the host C3000 solely. This second experiment aimed to show that without a specific biorecognition element on the surface it is impossible to detect live bacteria just by exposing the biosample to the functionalized surface.

In both experiments (Figs 5 and 6), it is clear that the minimum during bacteria incubation significantly shifts towards shorter wavelengths (green double curves). This is attributed to the high RI of the highly concentrated bacteria solution ( $10^8$  CFU/mL). However, after several washes in PBS, despite the very high concentration of the bacteria samples, no wavelength shift was observed, indicating that there is no interaction and no specific binding on the surface. The obtained results confirm our previous findings on the selectivity and reliability of the developed sensor.

## Conclusions

In this work, we show for the first time the capability for monitoring of the growth of a biofilm using a  $\mu$ MZI-based biosensor. The effect has been shown as a result of exposing the functionalized biosensor to different concentrations of live bacteria. On top of high RI sensitivity (over 15,000 nm/RIU), when using MS2 bacteriophages as recognition elements, the reported device allows for stable and specific label-free detection of alive *E. coli* C3000. The limit of detection of the demonstrated real-time measurements is as low as 100 CFU/mL. The reliability of the functionalized sensor is confirmed with two negative controls. Based on the presented results, it can be concluded that the spectral response is the manifestation of phenomena taking place on the surface of the sensor, and not in the RI of the analyte. During the experiments, the effects of the transitions between surface- and volume-related effects were observed. We believe that the non-monotonic trend in the spectral responses was a result of the investigated working point of the  $\mu$ MZI as well as the thickness of the bilayer. Due to its very high RI sensitivity, very low-temperature sensitivity and ability to investigate sub-nanoliter volumes, the sensor is well suited for future biological and chemical analysis.

## References

- Angus, D. C. & van der Poll, T. Severe Sepsis and Septic Shock. *N. Engl. J. Med.* **369**, 840–851 (2013).
- Newell, D. G. *et al.* Food-borne diseases - The challenges of 20years ago still persist while new ones continue to emerge. *Int. J. Food Microbiol.* **139**, S3–S15 (2010).
- Tait, E., Perry, J. D., Stanforth, S. P. & Dean, J. R. Bacteria detection based on the evolution of enzyme-generated volatile organic compounds: Determination of *Listeria monocytogenes* in milk samples. *Anal. Chim. Acta* **848**, 80–87 (2014).
- Brzozowska, E. *et al.* Recognition of bacterial lipopolysaccharide using bacteriophage-adhesin-coated long-period gratings. *Biosens. Bioelectron.* **67**, 93–99 (2015).
- Queirós, R. B., De-Los-Santos-Álvarez, N., Noronha, J. P. & Sales, M. G. F. A label-free DNA aptamer-based impedance biosensor for the detection of *E. coli* outer membrane proteins. *Sensors Actuators, B Chem.* **181**, 766–772 (2013).
- Interest, G. Response to questions posed by the food safety and inspection service regarding determination of the most appropriate technologies for the food safety and inspection service to adopt in performing routine and baseline microbiological analyses. *J. Food Prot.* **73**, 1160–1200 (2010).
- Smetana, M. *et al.* Detection of bacteria using bacteriophages as recognition elements immobilized on long-period fiber gratings. *Opt. Express* **19**, 7971 (2011).
- Kinet, D. *et al.* Fiber Bragg Grating Sensors toward Structural Health Monitoring in Composite Materials: Challenges and Solutions. *Sensors* **14**, 7394–7419 (2014).
- Jensen, J. B. *et al.* Photonic crystal fiber based evanescent-wave sensor for detection of biomolecules in aqueous solutions. *Opt. Lett.* **29**, 1974 (2004).
- Bandara, A. B. *et al.* Detection of methicillin-resistant staphylococci by biosensor assay consisting of nanoscale films on optical fiber long-period gratings. *Biosens. Bioelectron.* **70**, 433–440 (2015).
- Koba, M. *et al.* Bacteriophage adhesin-coated long-period grating-based sensor: Bacteria detection specificity. *J. Light. Technol.* **34**, 4531–4536 (2016).
- Chiniforooshan, Y. *et al.* Double resonance long period fiber grating for detection of *E. coli* in trace concentration by choosing a proper bacteriophage. **10323**, 103234X (2017).
- Wang, Y., Yang, M., Wang, D. N., Liu, S. & Lu, P. Fabricated By Femtosecond Laser Micromachining for Refractive Index Measurement With High Sensitivity. *J. Opt. Soc. Am. B* **27**, 370–374 (2010).
- Janik, M. *et al.* Sensitivity Pattern of Femtosecond Laser Mach-Zehnder Interferometers, as Applied to Small-Scale Refractive Index Sensing. *IEEE Sens. J.* **17**, 3316–3322 (2017).
- Hu, T. Y. & Wang, D. N. Optical fiber in-line Mach-Zehnder interferometer based on dual internal mirrors formed by a hollow sphere pair. *Opt. Lett.* **38**, 3036 (2013).
- Liao, C. R., Wang, D. N. & Wang, Y. Microfiber in-line Mach-Zehnder interferometer for strain sensing. *Opt. Lett.* **38**, 757–9 (2013).

17. Li, Z. *et al.* Highly-sensitive gas pressure sensor using twin-core fiber based in-line Mach-Zehnder interferometer. *Opt. Express* **23**, 6673 (2015).
18. Li, Z. *et al.* Label-free detection of bovine serum albumin based on an in-fiber Mach-Zehnder interferometric biosensor. *Opt. Express* **25**, 17105 (2017).
19. Pal, M. *et al.* Direct immobilization of antibodies on Zn-doped Fe<sub>3</sub>O<sub>4</sub> nanoclusters for detection of pathogenic bacteria. *Anal. Chim. Acta* **952**, 81–87 (2017).
20. Yazgan, I., Noah, N. M., Toure, O., Zhang, S. & Sadik, O. A. Biosensor for selective detection of E. coli in spinach using the strong affinity of derivatized mannose with fimbrial lectin. *Biosens. Bioelectron.* **61**, 266–273 (2014).
21. Ohk, S. H., Koo, O. K., Sen, T., Yamamoto, C. M. & Bhunia, A. K. Antibody-aptamer functionalized fibre-optic biosensor for specific detection of *Listeria monocytogenes* from food. *J. Appl. Microbiol.* **109**, 808–817 (2010).
22. Tripathi, S. M. *et al.* Long period grating based biosensor for the detection of *Escherichia coli* bacteria. *Biosens. Bioelectron.* **35**, 308–312 (2012).
23. Brewster, L., Langley, M. & Twa, D. Co-infection of C3000 *Escherichia coli* with Bacteriophages MS2 and, T7 or  $\Phi$  X-174 Results in Differential Cell Lysis Patterns. *J. Exp. Microbiol. Immunol.* **16**, 1–5 (2012).
24. Śmietana, M., Mysłiwiec, M., Mikulic, P., Witkowski, B. S. & Bock, W. J. Capability for fine tuning of the refractive index sensing properties of long-period gratings by atomic layer deposited Al<sub>2</sub>O<sub>3</sub> overlays. *Sensors (Switzerland)* **13**, 16372–16383 (2013).
25. Cras, J. J., Rowe-Taitt, C. A., Nivens, D. A. & Ligler, F. S. Comparison of chemical cleaning methods of glass in preparation for silanization. [Papers/1-s2.0-S0956566399000433-main.pdf](#) [Link]. *Biosens. Bioelectron.* **14**, 683–688 (1999).
26. Ebner, A., Hinterdorfer, P. & Gruber, H. J. Comparison of different aminofunctionalization strategies for attachment of single antibodies to AFM cantilevers. *Ultramicroscopy* **107**, 922–927 (2007).
27. Gopinath, S. C. B. *et al.* Surface functionalization chemistries on highly sensitive silica-based sensor chips. *Analyst* **137**, 3520 (2012).
28. Śmietana, M., Janik, M., Koba, M. & Bock, W. J. Transition between bulk and surface refractive index sensitivity of micro-cavity in-line Mach-Zehnder interferometer induced by thin film deposition. *Opt. Express* **25**, 26118–26123 (2017).
29. Śmietana, M., Mikulic, P. & Bock, W. J. Nano-coated long-period gratings for detection of sub-nanometric changes in thin-film thickness. *Sensors Actuators, A Phys.* **270**, 79–83 (2018).
30. Gunda, N. S. K., Singh, M., Norman, L., Kaur, K. & Mitra, S. K. Optimization and characterization of biomolecule immobilization on silicon substrates using (3-aminopropyl)triethoxysilane (APTES) and glutaraldehyde linker. *Appl. Surf. Sci.* **305**, 522–530 (2014).
31. Oceans, S. & Chromatogr, J. Light scattering by viral suspensions. 492–498 (1998).
32. Liu, P. Y. *et al.* An optofluidic imaging system to measure the biophysical signature of single waterborne bacteria. *Lab Chip* **14**, 4237–4243 (2014).
33. Rodrigues, D. F. & Elimelech, M. Role of type 1 fimbriae and mannose in the development of *Escherichia coli* K12 biofilm: From initial cell adhesion to biofilm formation. *Biofouling* **25**, 401–411 (2009).
34. Srinivasan, R., Umesh, S., Murali, S., Asokan, S. & Siva Gorthi, S. Bare fiber Bragg grating immunosensor for real-time detection of *Escherichia coli* bacteria. *J. Biophotonics* **10**, 224–230 (2017).
35. Li, Y. *et al.* Immobilized optical fiber microprobe for selective and sensitive *Escherichia coli* detection. *J. Biophotonics* **28**, e201700162 (2017).
36. Wandemur, G. *et al.* Plastic optical fiber-based biosensor platform for rapid cell detection. *Biosens. Bioelectron.* **54**, 661–666 (2014).
37. Bharadwaj, R. *et al.* Evanescent wave absorbance based fiber optic biosensor for label-free detection of E. coli at 280nm wavelength. *Biosens. Bioelectron.* **26**, 3367–3370 (2011).

## Acknowledgements

This work was supported by the National Science Centre (NCN) in Poland under grants No. 2014/13/B/ST7/01742, National Centre for Research and Development in Poland within Techmatstrateg grant No. 347324, the Natural Sciences and Engineering Research Council of Canada, and the Canada Research Chairs Program. Authors acknowledge the INRS-Institute Armand-Frappier Research Center for providing biological materials.

## Author Contributions

M.J. conceived and planned the experiments. M.J. and A.C. carried out the experiments. M.J., M.K. and M.Ś. contributed to the interpretation of the results. M.J., M.K., W.J.B. and M.Ś. worked on the manuscript.

## Additional Information

**Competing Interests:** The authors declare no competing interests.

**Publisher's note:** Springer Nature remains neutral with regard to jurisdictional claims in published maps and institutional affiliations.



**Open Access** This article is licensed under a Creative Commons Attribution 4.0 International License, which permits use, sharing, adaptation, distribution and reproduction in any medium or format, as long as you give appropriate credit to the original author(s) and the source, provide a link to the Creative Commons license, and indicate if changes were made. The images or other third party material in this article are included in the article's Creative Commons license, unless indicated otherwise in a credit line to the material. If material is not included in the article's Creative Commons license and your intended use is not permitted by statutory regulation or exceeds the permitted use, you will need to obtain permission directly from the copyright holder. To view a copy of this license, visit <http://creativecommons.org/licenses/by/4.0/>.

© The Author(s) 2018